Experimental investigation of parameter influence on synthetic jet vortex rings impinging onto a solid wall

Yang Xu[1], Jin-Jun Wang[1]*

[1] Key Laboratory of Fluid Mechanics, Beijing University of Aeronautics and Astronautics, Ministry of Education, Beijing, PR China

* jjwang@buaa.edu.cn

Abstract

This study conducts an experimental investigation of the effects of the stroke length and Reynolds number on the flow behavior of synthetic jet vortex rings impinging onto a solid wall. A two-dimensional time-resolved particle image velocimetry system is employed to measure the planar velocity field across the jet centerline. All the experiments have been performed at a constant orifice-to-wall distance (H_0/D_0 = 8.0), whereas three different stroke lengths (L_0/D_0 = 1.8, 3.6, and 7.2) and two Reynolds numbers (Re_{sj} = 111 and 333) are selected for comparison. With the help of the quantitative particle image velocimetry data, instantaneous wall pressure and wall shear stress distributions are evaluated simultaneously to link the dynamic vortical events in the vicinity of the wall with the wall fields. It is found that the stroke length effect on an impinging synthetic jet is mainly reflected in the vortex ring coherence before impacting the wall, whereas the effect of the Reynolds number on the flow behavior for a small stroke length is more significant than that for a large one.

1 Introduction

Synthetic jets are produced by an oscillating membrane or a piston to periodically blow and suck fluid through an existing exit, resulting in consecutive vortex rings by an orifice or vortex pairs by a slot in the downstream flow. During one oscillation cycle, the fluid ejected from the exit is equal to the inhaled, so synthetic jets are also named zero-net-mass-flux (ZNMF) jets (Cater and Soria (2002)). The flow characteristics of a synthetic jet are mainly determined by two non-dimensional parameters: the Reynolds number (Re_{sj}) and dimensionless stroke length (L)(Smith and Glezer (1998) and Glezer et al. (2005)). The former mainly decides the flow state and strength of synthetic jet vortices, and the latter is usually associated with the length of a fluid column ejected during the blowing cycle, i.e., the distance of the vortex ring/pair from the exit (Shuster and Smith (2007)).

Synthetic jets have a number of advantages over those that are continuous because of the output of the vortices mentioned above. Currently, synthetic jets have shown potential application in heat transfer in place of continuous jets impinging onto a heated wall, namely impinging synthetic jets. Pavlova and Amitay (2006) showed that the impinging synthetic jet is approximately three times more effective in cooling a heated wall than an impinging continuous jet. Additionally, they found that for a large orifice-to-wall distance, a low frequency impinging synthetic jet with is more effective than one with a high frequency. Conversely, when the orifice-to-wall distance is small, the high frequency synthetic jet performs better in removing heat because of the merging and breakdown of vortices before interacting with the wall. Arik (2007) conducted an experimental study on the heat transfer of small-scale synthetic jets by using infrared camera measurements. It was reported that, depending on the heater size, the synthetic jet enhances heat transfer from 4.5–10 times than that of natural convection. Gillespie et al. (2006) presented that the heat transfer rate can be maximized when the excitation frequency of the synthetic jet approximates the resonance frequency of the driving cavity. Persoons et al. (2011) compared heat transfers in the stagnation point between

impinging synthetic and continuous jets, and identified four heat transfer regimes for impinging synthetic jets based on the ratio of the stroke length to the orifice-to-wall distance. Chaudhari et al. (2011) compared the cooling performances of impinging synthetic jets of various exit shapes (i.e., square, circular and rectangular) having the same hydraulic diameter. Their results showed that the square exit promotes the highest heat transfer for longer orifice-to-wall distances, whereas a rectangular exit with aspect ratios from 3.0–5.0 yields the best cooling effect for shorter orifice-to-wall distances. Ghaffari et al. (2016) observed the degradation in the heat transfer effect of an impinging synthetic jet in short orifice-to-wall distances. They reported that the incomplete vortex growth and re-entrainment of warm fluid back into the jet flow causes heat transfer reduction.

Nevertheless, the knowledge of the basic flow feature of these jets is still limited as compared to their free development and heat transfer counterparts. To solve the problem of the lack of knowledge on the flow behavior surrounding impinging synthetic jets and to clarify the global flow dynamics of the synthetic jet/wall interaction, this study aims to investigate the flow characteristics and vortical structure evolutions of axisymmetric synthetic jets impinging onto a solid wall. Synthetic jets with three stroke lengths (L_0/D_0 = 1.8, 3.6, and 7.2) at two Reynolds numbers (Re_{sj} = 111 and 333) are investigated for a fixed orifice-to-wall distance (H_0/D_0 = 8.0). Through the PIV technique, the instantaneous wall pressure and wall shear stress are simultaneously evaluated to link dynamic vortical events with the distributions of the wall fields, which provide a better understanding of the vortex/wall interaction mechanism.

2 Experimental Setup

The experiment was conducted in a transparent water tank that is relatively similar to those that were successfully used by Xu et al. (2013), Xu and Wang (2016), and Xu et al. (2017), as shown in Figure 1. The water tank is made of plexiglass with a wall thickness of 20 mm. The tank size is 600 *mm* × 600 *mm* × 600 *mm*, whose dimensions were enough larger than the characteristic dimension of the synthetic jet (i.e., orifice diameter D_0 = 10 mm) in this study. Thus, this water tank is considered to be sufficiently large to provide a shield from outside interferences, and produce a quiet flow environment for this experiment. A 20-*mm* thick plexiglass flat plate was placed vertically in the tank as the impingement solid wall. The distance between the impingement wall and jet exit orifice (orifice-to-wall distance) was defined as H_0. Here, the synthetic jet vortex rings were generated by a piston-cylinder apparatus. Through a connecting rod, the piston was linked to an eccentric disk that is bolted to a servo motor, whereas the cylinder was connected to an "L-shaped" hollow circular cylinder by a Teflon tubing, as shown in Figure 1. So the motor rotation was transformed to the piston reciprocating motion, producing periodic vortex rings at the exit orifice of the "L-shaped" hollow circular cylinder. Based on the conservation of mass, the instantaneous fluid velocity ($v_o(t)$) at the orifice can be calculated by Eq. (1) using the actuator geometric parameters:

$$v_o(t) = -2\pi e f_0 \left(\frac{D_i}{D_0}\right)^2 \sin(2\pi f_0 t)\left(\frac{e\times\cos(2\pi f_0 t)}{\sqrt{l^2-(e\times\sin(2\pi f_0 t))^2}}+1\right) \tag{1}$$

where e is the eccentricity of the eccentric disk; D_i is the piston diameter; D_0 is the orifice diameter; l is the length of the connecting rod; f_0 is the excitation frequency. Considering that the length of the connecting rod (l = 300 mm) was much larger than the eccentricity (e_{max} = 4.4 mm), (e_{max}/l << 1), Eq. (1) can be simplified as Eq. (2):

$$v_o(t) \approx 2\pi e f_0 \left(\frac{D_i}{D_0}\right)^2 \sin(2\pi f_0 t) \tag{2}$$

Thus, the characteristic of the velocity of the synthetic jet (V_0), defined as the time-averaged blowing velocity over the entire jet cycle (Smith and Glezer (1998)), was calculated as:

$$V_0 = \frac{1}{T_0}\int_0^{T_0/2} v_o(t)\,dt = 2ef_0\left(D_i/D_0\right)^2 \tag{3}$$

where $T_0 = 1/f_0$ is the excitation period. Then, the dimensionless stroke length (L) and Reynolds number (Re_{sj}) of the synthetic jet were expressed as:

$$\mathrm{Re}_{sj} = \frac{V_0 D_0}{\nu} \tag{4}$$

$$L = \frac{L_0}{D_0} = \frac{V_0 T_0}{D_0} \tag{5}$$

where ν is the kinematic viscosity of water and $L_0 = V_0 T_0$ is the stroke length. The experimental parameters for all tested impinging synthetic jets are summarized in Table 1. Both the orifice diameter, D_0 =10 mm, and orifice-to-wall distance, H_0 = 80 mm, were maintained throughout the study.

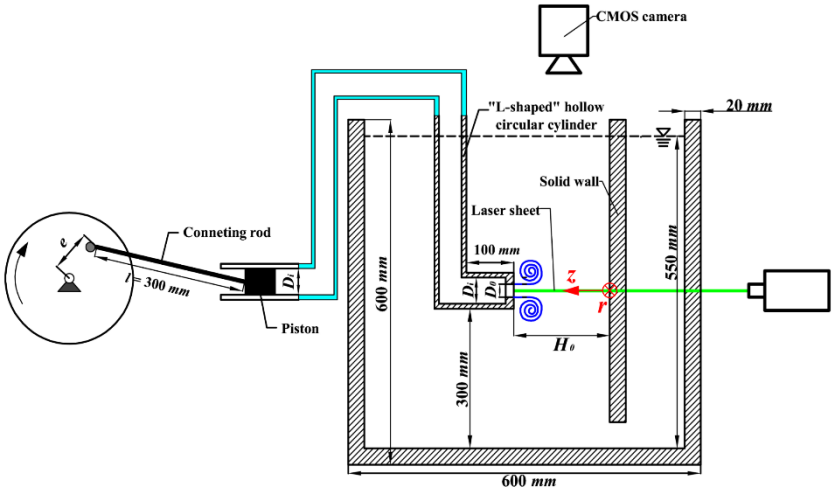

Figure 1: Experimental set-up.

Re_{sj}	e (mm)	f_0 (Hz)	D_0 (mm)	H_0 (mm)	L_0/D_0	L_0/H_0	St
111	1.1	0.60	10	80	1.8	0.225	3.48
	2.2	0.30	10	80	3.6	0.45	1.74
	4.4	0.15	10	80	7.2	0.90	0.87
333	1.1	1.80	10	80	1.8	0.225	3.48
	2.2	0.90	10	80	3.6	0.45	1.74
	4.4	0.45	10	80	7.2	0.90	0.87

Table 1: Experimental parameters for all tested cases

A time-resolved planar particle image velocimetry system was used to measure the fluid velocity. The water in the tank was seeded with hollow glass spheres. In the PIV system, the seeding particles were illuminated by a continuous 532 nm laser with an output power of 5 W. A laser sheet, approximately 1.0 *mm* thick, was adjusted to be positioned on a horizontal plane through the centerline, as depicted in Figure 1. So the flow information within a symmetric plane was recorded in the study. The laser sheet plane was defined as the experimental *r*-*z* coordinate plane with the coordinate origin chosen as the intersection of the jet centerline with the impingement wall. The *z*-axis (axial direction) was set along the jet centerline and directed towards the exit orifice, and the *r*-axis (radial direction) was set perpendicular to the *z*-axis, as shown in Figure 1. A high-speed CMOS camera (Photron FastcamSA2/86K-M3) with a Nikon macro lens (AF 105 mm/F2.8) was used to capture the particle images. The magnification of the particle image was set as 0.062 mm/pix. Thus, the captured field of view equaled approximately 95 *mm* × 85 *mm* ($9.5D_0 \times 8.5D_0$) in the radial and axial directions, respectively. A multi-pass interrogation algorithm was employed to obtain the velocity vectors. The final interrogation window was set as 32 × 32 pixels with an overlap rate of 50%. The particle image density was evaluated to be approximately 0.05 particles per pixel. Thus, on average, there were

approximately 50 image particles in the final interrogation window. For adopted particles (diameter approximately occupies 3 pixels), the uncertainty of the PIV-measured velocity was estimated to be less than 1% using 0.1 pixels as the subpixel peak-fitting uncertainty.

3 Results

Figure 2 shows the correlation coefficient of the axial velocity fluctuations as the function of the distance ($\Delta z/D_0$) between the referred and targeted points on the centerline. The reference point is located at z/D_0 = 7.8 on the centerline, which is close to the exit orifice. As shown in figure 2, all the correlation coefficient values for L_0/D_0 = 3.6 and 7.2 are relatively large from the exit orifice to the impingement wall at both tested Reynolds numbers. This result indicates that the synthetic jet vortex rings maintain coherence well during their convection to the wall for these two stroke lengths. However, the correlation coefficient for L_0/D_0 = 1.8 at Re_{sj} = 111 begins to greatly decrease from $\Delta z/D_0 \approx 4.8$, then reduces to a small value of approximately 0.1 at $\Delta z/D_0 \approx 3.0$, exhibiting a low correlation, as shown in Figure 2a. This observation indicates that the synthetic jet vortex rings have lost coherence before reaching the wall for this case. At a higher Re_{sj} (Re_{sj} = 333), Figure 2b depicts that the correlation coefficient of L_0/D_0 = 1.8 continuously decreases from the jet orifice until $\Delta z/D_0 \approx 1.0$, where it reaches a plateaus (approximately 0.15). This result illustrates that the synthetic jet vortex rings for this case appears to be in the transition state as they move towards the wall.

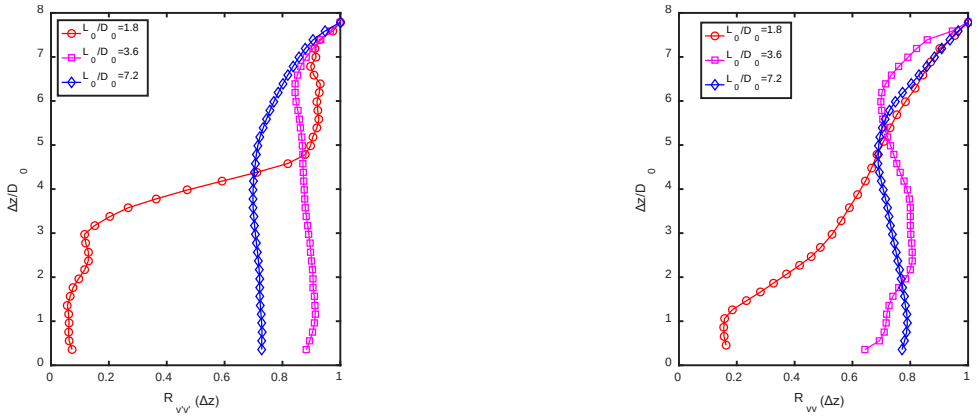

(a) (b)

Figure 2: Cross-correlation of axial velocity fluctuations along jet centerline at (a) Re_{sj}=111 and (b) Re_{sj}=333; (c) normalized radial profiles of axial mean velocity at z/D_0=4.0

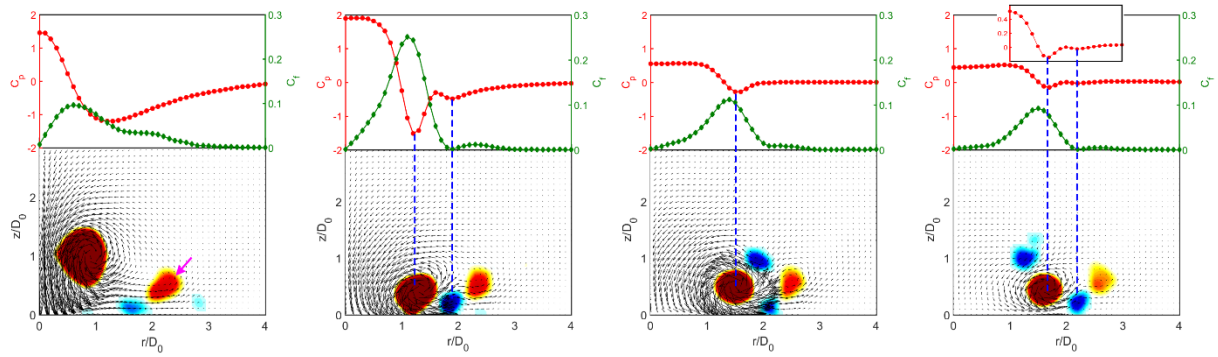

(a) t/T_0=0 (b) t/T_0=0.14 (c) t/T_0=0.27 (d) t/T_0=0.375

Figure 3: Time evolutions of wall pressure (C_p) and wall skin friction (C_f) coefficients for L_0/D_0=7.2 at Re_{sj}=333.

Wall field results show that the primary, secondary and tertiary vortex rings produce a negative peak in the wall pressure distribution around their vortex cores (Figure 3). Moreover, Figure 3(b) depicts that the skin

friction coefficient peak induced by the primary vortex ring, is followed by a sudden reduction that implys a separation of the wall shear layer. Particularly, both the wall pressure and wall shear stress behavior for the smallest L_0/D_0 (L_0/D_0 =1.8) show no apparently time-periodic feature (Figure 4), similar to a steady impinging jet. This result is due to the fact that the synthetic jet vortex rings in this case lose coherence as convecting to the impingement wall.

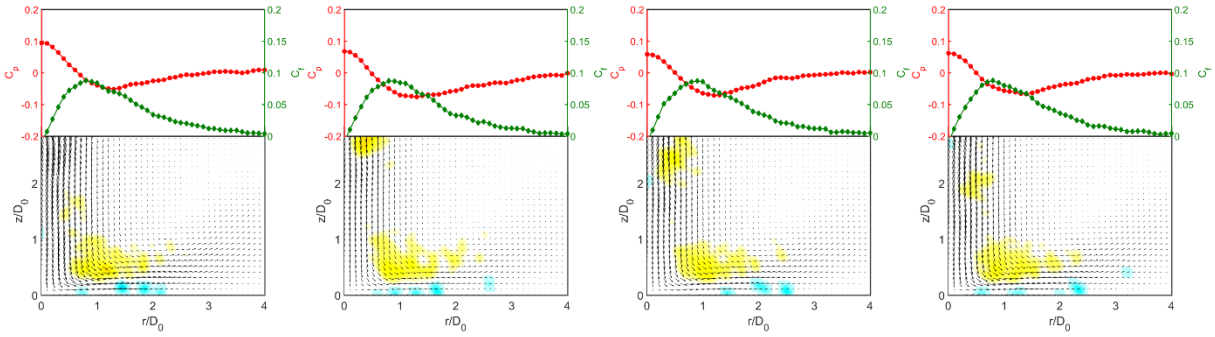

(a) t/T_0=0 (b) t/T_0=0.25 (c) t/T_0=0.5 (d) t/T_0=0.75

Figure 4: Time evolutions of wall pressure (C_p) and wall skin friction (C_f) coefficients for L_0/D_0=1.8 at Re_{sj}=111.

4 Conclusion

The steady and unsteady flow behavior of an impinging synthetic jet was investigated for three different stroke lengths at two Reynolds numbers using time-resolved PIV measurements. It is found that at a lower Reynolds number (Re_{sj} = 111), the synthetic jet is laminar, so viscous diffusion and dissipation cause the primary vortex ring to lose coherence as it approaches the wall for the smallest stroke length. However, as the Reynolds number increases to 333, the synthetic jet vortex rings for the smallest stroke length (L_0/D_0 = 1.8) gradually lose identity and transition to a turbulent jet before impacting the wall. This change in the flow morphology leads to a double peak distribution of the axial velocity, an enhancement in the velocity fluctuations, and a reduction of the radial velocity decay on the wall. It is concluded that the influence of the Reynolds number on the flow behavior of an impinging synthetic jet for a small stroke length is more significant than that for a large one.

Wall field evaluations illustrate that the near-wall flow structures have significant effects on the distributions of both the wall pressure and wall shear stress. Specifically, for the large stroke length (L_0/D_0 =3.6 and 7.2), the primary, secondary, and tertiary vortex rings can produce negative peaks in the wall pressure around their vortex cores. The peak of the skin friction coefficient induced by the primary vortex ring, is followed by a sudden reduction that indicates a separation of the wall shear layer. Particularly, it was found that the wall field (i.e., wall pressure and wall shear stress) behavior for the smallest stroke length (L_0/D_0 = 1.8) shows no apparent time-periodic feature at both Reynolds numbers, similar to a steady impinging jet. This observation can be attributed to the synthetic jet vortex rings that lose coherence before interacting with the wall. Furthermore, the viscous effect should be responsible for the incoherent vortex rings at a lower Re_{sj}, whereas at a higher Re_{sj}, the incoherence of the vortex rings is mainly caused by the transition.

Acknowledgements

This work is financially supported by the National Natural Science Foundation of China (grant no. 11721202), National Postdoctoral Program for Innovative Talents in China (BX201700018) and China Postdoctoral Science Foundation Grant (2018M630055).

References

Cater JE and Soria J (2002) The evolution of round zero-net-mass-flux jets. *Journal of Fluid Mechanics* 472: 167-200

Glezer A, Amitay M and Honohan A (2005) Aspects of low and high frequency actuation for aerodynamic flow control. *AIAA Journal* 43: 1501-1511

Smith BL and Glezer A (1998) The formation and evolution of synthetic jets. *Physics of Fluids* 10: 2281-2297

Shuster JM and Smith DR (2007) Experimental study of the formation and scaling of a round synthetic jet. *Physics of Fluids* 19: 045109

Pavlova A and Amitay M (2006) Electronic cooling using synthetic jet impingement. *Journal of Heat Transfer-ASME* 128: 897-907

Arik M (2007) An investigation into feasibility of impingement heat transfer and acoustic abatement of meso scale synthetic jets. *Applied Thermal. Engineering* 27(8): 1483-1494

Gillespie MB, Black WZ, Rinehart C and Glezer CA (2006) Local convective heat transfer from a constant heat flux flat plate cooled by synthetic air jets. *Journal of Heat Transfer-ASME* 128(10): 990-1000

Persoons T, McGuinn A and Murray DB (2011) A general correlation for the stagnation point Nusselt number of an axisymmetric impinging synthetic jet. *International Journal of Heat and Mass Transfer* 54 (17): 3900-3908

Chaudhari M, Puranik B and Agrawal A (2011) Multiple orifice synthetic jet for improvement in impingement heat transfer. *International Journal of Heat and Mass Transfer* 54(9): 2056-2065

Ghaffari O, Solovitz SA and Arik M (2016) Investigation into flow and heat transfer for a slot impinging synthetic jet. *International Journal of Heat and Mass Transfer*100: 634-645

Xu Y, Feng LH and Wang JJ (2013) Experimental investigation of a synthetic jet impinging on a fixed wall. *Experiments in Fluids* 54(5): 1512

Xu Y and Wang JJ (2016) Flow structure evolution for laminar vortex rings impinging onto a fixed solid wall. *Experimental Thermal and Fluid Science* 75: 211-219

Xu Y, Wang JJ, Feng LH, He GS and Wang ZY (2018) Laminar vortex rings impinging onto porous walls with a constant porosity. *Journal of Fluid Mechanics* 837:729-764